Available online at www.sciencedirect.com
SCIENCE DIRECT®
Journal of Sound and Vibration 268 (2003) 555–580
JOURNAL OF SOUND AND VIBRATION
www.elsevier.com/locate/jsvi

Application of generalized complex modes to the calculation of the forced response of three-dimensional poroelastic materials

O. Dazel[a], F. Sgard[a], C.-H. Lamarque[b,*]

[a] *Laboratoire des Sciences de l'Habitat (LASH), DGCB URA CNRS 1652, Ecole Nationale des Travaux Publics de l'Etat, Rue Maurice Audin, F-69518 Vaulx-en-Velin, Cedex, France*

[b] *Laboratoire Géo-Matériaux (LGM), DGCB URA CNRS 1652, Ecole Nationale des Travaux Publics de l'Etat, Rue Maurice Audin, F-69518 Vaulx-en-Velin, Cedex, France*

Received 27 May 2002; accepted 18 November 2002

Abstract

Finite element models based on Biot's $\{\mathbf{u}, P\}$ formulation for poroelastic materials are widely used to predict the behaviour of structures involving porous media. The numerical solution of such problems requires however important computational resources and the solution algorithms are not optimized. To improve the solution process, a modal approach based on an extension of the complex modes technique has been proposed recently and applied successfully to a simplified mono-dimensional problem. In this paper, this technique is investigated in the case of three-dimensional poroelastic problems. The technique is first recalled, then analytical proof of the stability of the model are given followed by considerations of numerical improvements of the method. An energetic interpretation of the generalized complex modes is then given and some numerical results are presented to illustrate the performance of the approach.

1. Introduction

Porous materials are commonly used in many applications in the fields of aeronautics, automobile, civil engineering and buildings because of their interesting properties of absorption of either acoustical waves or mechanical energy. The dynamical behaviour of such materials can be well predicted by using the Biot/Allard formulation [1–4]. Several other formulations [5–9] have been proposed to calculate the vibroacoustic behaviour of multilayered structures involving these media. Among them, Panneton and Atalla [7] presented a finite-element formulation based on the $\{\mathbf{u}, \mathbf{U}\}$ displacement formalism. Mixed $\{\mathbf{u}, P\}$ formulations have then been undertaken. Atalla

*Corresponding author. Tel.: +33-4-72-04-70-75; fax: +33-4-72-04-71-56.
E-mail address: claude.lamarque@entpe.fr (C.-H. Lamarque).

0022-460X/03/$ - see front matter
doi:10.1016/S0022-460X(03)00373-0

et al. [10] and Debergue et al. [11] proposed a weak integral formulation for a mixed pressure–displacement version of Biot's poroelasticity equations for harmonic time dependencies and its finite-element discretization. This $\{\mathbf{u}, P\}$ formulation is adopted in the rest of this paper.

Nevertheless, the main drawback of the finite-element techniques applied to poroelastic materials lies in the large size of the linear systems to be solved. To improve the solving process, different solutions have been investigated. Some of them consisted of improving the convergence of the finite-element approach like hierarchical elements [12,13] or high order Lagrange elements [14] or to use other basis functions to express the solution like a mixed wave finite element method [15]. Another set of techniques relies on modal analysis. However, the application of classical modal techniques to the mixed $\{\mathbf{u}, P\}$ finite-element problem is prohibited by the non-linear frequency dependency of the associated eigenvalue problem. Simplified modal techniques have been introduced [16,17]. Nevertheless, none of these approaches leads to a significant reduction of the number of degrees of freedom, particularly for three-dimensional configurations.

Recently, Dazel et al. [18] proposed a generalized complex mode technique for poroelastic problems and applied it to a simplified finite-element mono-dimensional problem. This technique consists of making a Taylor expansion of the frequency-dependant coefficients of the model and then solving the associated eigenvalue problem in a generalized state space extending the one introduced by Duncan et al. [19]. It has been shown that this technique allows for the convergence of the solution and yields a significant reduction of the number of degrees of freedom of the problem. Preliminary investigations of a numerical convergence criterion have also been carried out.

The purpose of this paper is to investigate the performance of the complex modal technique in the calculation of the forced response of three-dimensional porous materials. The main contributions of this paper are an analytical proof of the stability of the solution, numerical improvements of the method, an energetic interpretation of generalized complex modes and a presentation of three-dimensional applications. Section 2 recalls the finite-element poroelastic problem together with the generalized complex mode technique as introduced in Ref. [18]. Section 3 presents theoretical arguments of the stability of the solution and Section 4 deals with numerical improvements of this technique, which are specific to the poroelastic problem. More particularly, Section 5 is devoted to the energetic analysis of generalized complex modes and Section 6 deals with the convergence of the procedure in the case of three-dimensional poroelastic problems. Section 7 concludes the paper.

2. Generalized complex mode technique

2.1. The original poroelastic problem

The finite-element problem associated with the harmonic forced response of a porous material at circular frequency ω is given by Atalla et al. [10]

$$\begin{bmatrix} (1+\mathrm{j}\eta_s)[\mathbf{K}_{int}] + (\mathrm{j}\omega)^2\tilde{\rho}[\mathbf{M}_{int}] & -\tilde{\gamma}[\mathbf{C}_{int}] \\ -\omega^2\tilde{\gamma}[\mathbf{C}_{int}]^{\mathrm{t}} & \dfrac{h^2}{\widetilde{\rho_{22}}}[\mathbf{H}_{int}] - \omega^2\dfrac{h^2}{\tilde{R}}[\mathbf{Q}_{int}] \end{bmatrix} \begin{Bmatrix} \mathbf{u} \\ \mathbf{P} \end{Bmatrix} \mathrm{e}^{\mathrm{j}\omega t} = \begin{Bmatrix} \mathbf{F}^s \\ \mathbf{F}^f \end{Bmatrix} \mathrm{e}^{\mathrm{j}\omega t}. \tag{1}$$

u is the displacement nodal vector of the solid phase, and **P** is the interstitial pressure nodal vector of the fluid phase. $\mathbf{F}^s$ and $\mathbf{F}^p$ are, respectively, the forcing applied to the solid and to the fluid phase. h denotes the porosity. The effective densities $\tilde{\rho}$, $\widetilde{\rho_{22}}$ and the coupling coefficient $\tilde{\gamma}$ are given by Atalla et al. [10]. η_s is the structural damping coefficient and $\tilde{R}$ may be interpreted as the bulk modulus of the air occupying a fraction h of a unit volume of aggregate. $[\mathbf{K}_{int}]$, $[\mathbf{M}_{int}]$ are, respectively, associated with the stiffness and mass matrices of the solid phase. $[\mathbf{H}_{int}]$ and $[\mathbf{Q}_{int}]$ are, respectively, associated with the kinetic and compression energy matrices of the fluid phase. $[\mathbf{C}_{int}]$ is a coupling matrix between the solid and fluid phase. The definition of these matrices are given in Ref. [10]. Superscript "~" represents the complex frequency dependencies of the coefficients induced by both the constitutive laws and the specific $\{\mathbf{u}, P\}$ formulation.

2.2. Presentation of the technique

First of all, and for the sake of clarity, the headlines of the technique needed to understand this paper are presented. Details can be found in Ref. [18]. This technique is divided in four parts: the construction of the augmented problem, the mode computation, the projection of the problem on the modal family and the solving of the modal problem.

The purpose of the generalized complex mode technique is to approach the modes of a frequency-dependent operator $\mathscr{D}$ which can be written as

$$\mathscr{D}\mathbf{u} = \sum_{i=0}^{d} [\mathbf{M}_i](\mathrm{j}\omega)^i\mathbf{u} + \mathscr{R}_d\mathbf{u} = \mathscr{D}_d\mathbf{u} + \mathscr{R}_d\mathbf{u}. \tag{2}$$

$\mathscr{D}_d$ is called the expansion of operator $\mathscr{D}$, $\mathscr{R}_d$ is called the remainder where d corresponds to the order of Taylor expansions in terms of ω. Problem (1) can be expressed in the previous form by noting that

$$\tilde{\rho}[\mathbf{M}_{int}] = \sum_{i=0}^{d} m_i(\mathrm{j}\omega)^i[\mathbf{M}_{int}] + O(\omega^{d+1}), \quad [\mathbf{K}_{int}] = \sum_{i=0}^{d} k_i(\mathrm{j}\omega)^i[\mathbf{K}_{int}] + O(\omega^{d+1}), \tag{3a}$$

$$\frac{1}{\widetilde{\rho_{22}}}[\mathbf{H}_{int}] = \sum_{i=0}^{d} h_i(\mathrm{j}\omega)^i[\mathbf{H}_{int}] + O(\omega^{d+1}), \quad \frac{1}{\tilde{R}}[\mathbf{Q}_{int}] = \sum_{i=0}^{d} q_i(\mathrm{j}\omega)^i[\mathbf{Q}_{int}] + O(\omega^{d+1}), \tag{3b}$$

$$\tilde{\gamma}[\mathbf{C}_{int}] = \sum_{i=0}^{d} c_i(\mathrm{j}\omega)^i[\mathbf{C}_{int}] + O(\omega^{d+1}), \tag{3c}$$

where m_i, h_i, q_i and c_i are the coefficients of the Taylor expansions of $\tilde{\rho}$, $h^2/\tilde{\rho}_{22}$, $h^2/\tilde{R}$ and $\tilde{\gamma}$, respectively. As in Ref. [18] the structural damping is omitted in the step of calculation of modes. $[\tilde{\mathbf{K}}]$ is then equal to $[\mathbf{K}_{int}]$ so that $k_0 = 1$ and $k_i = 0$ for $i \in \mathbb{N}^*$. Hence, for the poroelastic problem, all these coefficients are real.

Eq. (1) can then be rewritten as

$$\sum_{i=0}^{d} [\mathbf{M}_i](\mathrm{j}\omega)^i \begin{Bmatrix} \mathbf{u} \\ \mathbf{P} \end{Bmatrix} + [\mathscr{R}_d](\omega) \begin{Bmatrix} \mathbf{u} \\ \mathbf{P} \end{Bmatrix} = \begin{Bmatrix} \mathbf{F}_s \\ \mathbf{F}_p \end{Bmatrix}. \tag{4}$$

The different matrices $[\mathbf{M}_i]$ are given by

$$[\mathbf{M}_0] = \begin{bmatrix} [\mathbf{0}] & [\mathbf{0}] \\ [\mathbf{0}] & -h_0[\mathbf{H}_{int}] \end{bmatrix}, \tag{5}$$

$$[\mathbf{M}_1] = \begin{bmatrix} [\mathbf{0}] & [\mathbf{0}] \\ [\mathbf{0}] & -h_1[\mathbf{H}_{int}] \end{bmatrix}, \tag{6}$$

$$[\mathbf{M}_2] = \begin{bmatrix} k_0[\mathbf{K}_{int}] & -c_0[\mathbf{C}_{int}] \\ -c_0[\mathbf{C}_{int}]^{\mathrm{t}} & -h_2[\mathbf{H}_{int}] - q_0[\mathbf{Q}_{int}] \end{bmatrix}, \tag{7}$$

$$[\mathbf{M}_3] = \begin{bmatrix} [\mathbf{0}] & -c_1[\mathbf{C}_{int}] \\ -c_1[\mathbf{C}_{int}]^{\mathrm{t}} & -h_3[\mathbf{H}_{int}] - q_1[\mathbf{Q}_{int}] \end{bmatrix}, \tag{8}$$

$$[\mathbf{M}_i] = \begin{bmatrix} m_{i-4}[\mathbf{M}_{int}] & -c_{i-2}[\mathbf{C}_{int}] \\ -c_{i-2}[\mathbf{C}_{int}]^{\mathrm{t}} & -h_i[\mathbf{H}_{int}] - q_{i-2}[\mathbf{Q}_{int}] \end{bmatrix} \quad (i \geqslant 4). \tag{9}$$

Each $[\mathbf{M}_i]$ is a real symmetric matrix and $[\mathscr{R}_d](\omega)$ is a matrix depending on ω and corresponding to the remainder.

The modes of $\mathscr{D}_d$ can then be calculated using the generalized unknown vector $\mathbf{U}$ defined as follows

$$\mathbf{U} = \begin{Bmatrix} (\mathrm{j}\omega)^{d-1}\mathbf{u} \\ \vdots \\ (\mathrm{j}\omega)\mathbf{u} \\ \mathbf{u} \end{Bmatrix}. \tag{10}$$

This construction is a generalization of Duncan's transformation [19]. Then, a classical modal problem can be written

$$[\mathbf{A}]\mathbf{U} = (\mathrm{j}\omega)[\mathbf{B}]\mathbf{U}, \tag{11}$$

with

$$[\mathbf{A}] = \begin{bmatrix} [\mathbf{L}] & [\mathbf{M}_0] \\ [\mathbf{\Gamma}] & [\mathbf{0}] \end{bmatrix} \quad \text{and} \quad [\mathbf{B}] = \begin{bmatrix} -[\mathbf{M}_d] & [\mathbf{0}] \\ [\mathbf{0}] & [\mathbf{\Gamma}] \end{bmatrix}, \tag{12}$$

where

$$[\mathbf{L}] = \begin{bmatrix} [\mathbf{M}_{d-1}] & \cdots & [\mathbf{M}_1] \end{bmatrix}, \tag{13}$$

and $[\mathbf{\Gamma}]$ is a $(n(d-1), n(d-1))$ matrix of trivial equations. It is possible to choose $[\mathbf{\Gamma}]$ in order to make $[\mathbf{A}]$ and $[\mathbf{B}]$ symmetric [18].

For the numerical implementation, it has been shown that, in the case where $[\mathbf{M}_d]$ is invertible, problem (11) can be written as

$$[\mathbf{C}]\mathbf{U} = \begin{bmatrix} -[\mathbf{M}_d]^{-1}[\mathbf{L}] & -[\mathbf{M}_d]^{-1}[\mathbf{M}_0] \\ [\mathbf{I}_{n(d-1)}] & [\mathbf{0}] \end{bmatrix} \mathbf{U} = (\mathrm{j}\omega)\mathbf{U}, \tag{14}$$

where $[\mathbf{I}_{n(d-1)}]$ denotes the identity matrix of order $n(d-1)$. It means that the dimension of the eigenvalue problem is equal to the product of the initial dimension of the system by the order of the expansion. Once the problem is constructed (first step), the first "m" modes of $\mathscr{D}_d$, noted $[\underline{\boldsymbol{\Phi}}]_m$, are computed (second step).

The solution of the problem in terms of modal coordinates is then undertaken. It has been shown [18] that the projection on the $[\underline{\boldsymbol{\Phi}}]_m$ family (third step) is equivalent to the projection on the $[\underline{\boldsymbol{\psi}}]_m$ one, where

$$[\underline{\boldsymbol{\Phi}}]_m = [[\underline{\boldsymbol{\psi}}]_m^{\mathrm{t}}[\underline{\boldsymbol{\Lambda}}]_m^{d-1}, \ldots [\underline{\boldsymbol{\psi}}]_m^{\mathrm{t}}[\underline{\boldsymbol{\Lambda}}]_m, [\underline{\boldsymbol{\psi}}]_m^{\mathrm{t}}]^{\mathrm{t}}, \tag{15}$$

where $[\underline{\boldsymbol{\Lambda}}]_m$ is the diagonal matrix of eigenvalues associated with the $[\underline{\boldsymbol{\psi}}]_m$ family. This allows for projecting the initial problem $\mathscr{D}\mathbf{u} = \mathbf{f}$ on the modal sub-family $[\underline{\boldsymbol{\psi}}]_m$ instead of $[\boldsymbol{\Phi}]_m$ thereby reducing the computational cost associated to the projection process. The last step is the solution of the problem of size m:

$$[\underline{\boldsymbol{\psi}}]_m^{\mathrm{t}}\mathscr{D}[\underline{\boldsymbol{\psi}}]_m\mathbf{z} = [\underline{\boldsymbol{\psi}}]_m^{\mathrm{t}}\mathbf{f}. \tag{16}$$

$\mathbf{z}$ corresponds to the vector of modal contributions. The value of m governs the convergence of the model. A criterion to select this value allowing for the convergence of the solution has been proposed. It consists of giving, for a considered configuration, a critical frequency ω_c and to select only the modes whose imaginary part of the eigenvalue ω_i is lower than this critical frequency. This critical frequency depends on the configuration, the loads and the maximum frequency of the spectrum of excitation ω_{max}. An adimensional coefficient α_c is introduced so that $\omega_c = \alpha_c\omega_{max}$. The procedure of determination of α_c is presented in Ref. [18] together with numerical applications.

3. Stability of the solution

In the previous paper [18], the stability of the solution was not justified analytically. The aim of this section is to prove it in the case of the poroelastic problem. This will show that the real part of all the eigenvalues are negative and then ensure that the related modes are stable. As the $\{\mathbf{u}, \mathbf{U}\}$ formulation is more suitable to prove the stability, the proof consists in expressing the generalized eigenvalue problem in the $\{\mathbf{u}, \mathbf{U}\}$ formalism. Further calculations presented in Appendices A, B and C allows one to simplify this problem and to finally prove the stability of the algorithm.

Let $(s, \{\mathbf{u}\atop\mathbf{P}\})$ be a solution of the generalized $\{\mathbf{u}, P\}$ eigenvalue problem (4) with $s = s_r + \mathrm{j}s_i$. This solution is such that

$$\begin{bmatrix} s^2[\mathbf{K}_{int}] + s^4\hat{\rho}\,[\mathbf{M}_{int}] & -s^2\hat{\gamma}\,[\mathbf{C}_{int}] \\ \hat{\gamma}[\mathbf{C}_{int}]^{\mathrm{t}} & \dfrac{h^2}{s^2}\dfrac{\hat{1}}{\rho_{22}}[\mathbf{H}_{int}] + h^2\dfrac{\hat{1}}{R}[\mathbf{Q}_{int}] \end{bmatrix} \begin{Bmatrix} \mathbf{u} \\ \mathbf{P} \end{Bmatrix} = \mathbf{0}. \tag{17}$$

The "^" symbols correspond to the expansions of the corresponding tilded coefficients. For example, the expression of $\hat{\rho}$ is given by

$$\hat{\rho} = \sum_{i=0}^{n_\rho} m_i s^i. \tag{18}$$

n_ρ is the order of the expansion of $\tilde{\rho}$ used for the construction of the modal problem. Hence, one gets the expansions of : $\hat{\rho} = \widehat{\rho_{11}} - \widehat{\rho_{12}^2/\rho_{22}}$, $\widehat{1/\rho_{22}}$, $\widehat{1/R}$ and $\hat{\gamma} = h\widehat{\rho_{12}/\rho_{22}} - h\widehat{Q/R}$.

Let U be the equivalent modal fluid displacement field defined by

$$-h\frac{\hat{1}}{\rho_{22}}\nabla P = s^2 U + s^2\frac{\widehat{\rho_{12}}}{\rho_{22}}u. \tag{19}$$

Like all the quantities defined in this section, U is deduced from the calculated modal fields and the expressions of the coefficients which were calculated for the expansion of the modal problem for the $\{\mathbf{u}, P\}$ formulation. U corresponds to the equivalent modal displacement of the fluid phase for the considered modal problem. Similarly, the modal stress tensor of the solid phase $\boldsymbol{\sigma}^s\widehat{(u, U)}$ and of the fluid phase $\boldsymbol{\sigma}^f\widehat{(u, U)}$ defined by the modal constitutive laws deduced from both stress–strain relation in harmonic motion and the expanded coefficients are now introduced

$$\frac{\hat{1}}{R}\boldsymbol{\sigma}^s\widehat{(u, U)} = \frac{\hat{A}}{R}\nabla\cdot u\mathbb{I} + 2\frac{\hat{1}}{R}N\boldsymbol{\epsilon}^s(u) + \frac{\hat{Q}}{R}\nabla\cdot U\mathbb{I}, \tag{20a}$$

$$\frac{\hat{1}}{R}\boldsymbol{\sigma}^f\widehat{(u, U)} = \nabla\cdot U\mathbb{I} + \frac{\hat{Q}}{R}\nabla\cdot u\mathbb{I}. \tag{20b}$$

$\mathbb{I}$ denotes the identity tensor. For memory, $\tilde{A}$ and N correspond to Lamé's coefficients for elastic solids. $\tilde{A}$ is given by

$$\tilde{A} = \frac{(1-h)}{h}\tilde{Q} + 2N\frac{v}{(1-2v)}, \tag{21}$$

v is the Poisson coefficient and N is the shear modulus. One gets

$$\frac{\hat{A}}{R} = \frac{(1-h)^2}{h^2} + \frac{\hat{1}}{R}2N\frac{v}{(1-2v)}. \tag{22}$$

The in vacuo stress tensor of the solid phase $\breve{\boldsymbol{\sigma}}^s(u)$ is then deduced from both modal stress tensors by

$$\breve{\boldsymbol{\sigma}}^s(u) = \boldsymbol{\sigma}^s\widehat{(u, U)} - \frac{\hat{Q}}{R}\boldsymbol{\sigma}^f\widehat{(u, U)}. \tag{23}$$

If the first block row of Eq. (17) is pre-multiplied by $(1/s^2)\widehat{1/\rho_{22}}\mathbf{u}^*$ and the second block row by $\overline{\widehat{(1/\rho_{22})}}\mathbf{P}^*$ (the symbol $^-$ denotes the conjugate), the equations of the solid and fluid phase are, respectively, given by

$$\frac{\hat{1}}{\rho_{22}}\mathbf{u}^*[\mathbf{K}_{int}]\mathbf{u} + s^2\frac{\hat{1}}{\rho_{22}}\hat{\rho}\mathbf{u}^*[\mathbf{M}_{int}]\mathbf{u} - \frac{\hat{1}}{\rho_{22}}\hat{\gamma}\mathbf{u}^*[\mathbf{C}_{int}]\mathbf{P} = 0, \tag{24}$$

$$\frac{\bar{\hat{1}}}{\rho_{22}}\hat{\gamma}\mathbf{P}^*[\mathbf{C}_{int}]^{\mathrm{t}}\mathbf{u} + \frac{h^2}{s^2}\frac{\hat{1}}{\rho_{22}}\frac{\bar{\hat{1}}}{\rho_{22}}\mathbf{P}^*[\mathbf{H}_{int}]\mathbf{P} + h^2\frac{\bar{\hat{1}}}{\rho_{22}}\frac{\hat{1}}{R}\mathbf{P}^*[\mathbf{Q}_{int}]\mathbf{P} = 0. \tag{25}$$

Eqs. (24) and (25) are combined (details can be found in Appendix A) in order to obtain the following relation

$$-\Gamma_{kin} + \Gamma_{def} = 0, \tag{26a}$$

where

$$\Gamma_{kin} = -s^2 \int_\Omega \underbrace{\left(\widehat{\rho'_{11}} u^* u + \widehat{\rho_{22}} \frac{\widehat{\rho_{12}}}{\rho_{22}} (u^* U + U^* u) + \widehat{\rho_{22}} U^* U \right)}_{\mathscr{I}_k} \mathrm{d}\Omega, \tag{26b}$$

and

$$\Gamma_{def} = \int_\Omega \underbrace{(\boldsymbol{\sigma}^s(\widehat{u, U}) : \boldsymbol{\epsilon}^s(u^*) + \boldsymbol{\sigma}^f(\widehat{u, U}) : \boldsymbol{\epsilon}^f(U^*))}_{\mathscr{I}_{def}} \mathrm{d}\Omega. \tag{26c}$$

The following quantities have been introduced

$$\widehat{\rho'_{11}} = \widehat{\rho_{11}} + \widehat{\rho_{22}} \left(\frac{\widehat{\rho_{12}}}{\rho_{22}} \right)^2 - \frac{\widehat{\rho_{12}^2}}{\rho_{22}}, \quad \widehat{\rho_{22}} = \left(\frac{\hat{1}}{\rho_{22}} \right)^{-1}. \tag{27}$$

Note that Γ_{kin} and Γ_{def} correspond just to notations introduced in the calculation. Their physical interpretation is hazardous when s is complex valued. However, it is possible to interpret them physically when the eigenvalue s is purely imaginary that is s is replaced by $\mathrm{j}\omega$. With this assumption, the real part of Γ_{kin} can be interpreted as twice the modal kinetic energy of the porous and the imaginary part as twice the modal energy dissipated through viscous damping. The real part of Γ_{def} represents twice the modal deformation energy of the porous and the imaginary part twice the modal energy dissipated through thermal damping. The simplification of $\mathscr{I}_k$ and $\mathscr{I}_{def}$ detailed in Appendices B and C leads to the rewriting of Eq. (26a) as

$$s^2 m(s) + s(c_{kin}(s) + c_d) + k_0 + r_k(s) + \mathrm{j} i_k(s) = 0, \tag{28}$$

with m and c_{kin} functions of s with a positive real part and an imaginary part in $O|s/H|^2$. k_0 and c_d pertains to $\mathbb{R}^+$ and both real functions of r_k and i_k are in $O|s/H'|^2$. H and H' are the characteristic viscous and thermal circular frequencies introduced by Panneton [16].

These functions are split into real and imaginary parts such that $m(s) = m_r(s) + \mathrm{j} m_i(s)$, $c_{kin}(s) + c_d = c_r(s) + \mathrm{j} c_i(s)$ and $k_0 + r_k(s) + \mathrm{j} i_k(s) = k_r(s) + \mathrm{j} k_i(s)$. One has $m_r(s) > 0$, $c_r(s) > 0$, $k_r(s) > 0$ and the Landau's relations, $m_i(s) = O|s/H|^2$, $c_i(s) = O|s/H|^2$ and $k_i(s) = O|s/H'|^2$. The real and imaginary parts of Eq. (28) can then be separated. Hence,

$$(s_r^2 - s_i^2) m_r(s) - 2 s_r s_i m_i(s) + s_r c_r(s) - s_i c_i(s) + k_r(s) = 0, \tag{29a}$$

$$2 s_r s_i m_r(s) + (s_r^2 - s_i^2) m_i(s) + s_r c_i(s) + s_i c_r(s) + k_i(s) = 0. \tag{29b}$$

The Landau's relations on m_i, c_i and k_i indicate that $2 s_r s_i m_i(s) = o((s_r^2 - s_i^2) m_r(s))$, $s_r c_i(s) = o(s_i c_r(s))$, $s_i c_i(s) = o(s_r c_r(s))$ and $k_i(s) = o(2 s_r s_i m_r(s))$. This allows one to neglect the corresponding terms and Eq. (29b) gives

$$s_i (2 s_r m_r(s) + c_r(s)) = 0. \tag{30}$$

Hence, if $s_i \neq 0$, one has $s_r < 0$. If not, Eq. (29a) is rewritten

$$\underbrace{s_r^2 m_r(s)}_{\in \mathbb{R}^+} + s_r c_r(s) + \underbrace{k_r(s)}_{\in \mathbb{R}^+} = 0, \tag{31}$$

which indicates that $s_r < 0$. The stability of the solution is then ensured.

4. Numerical improvements of the method

This section is devoted to the numerical implementation of this technique applied to three-dimensional finite-element poroelastic problems. It relies on a special hypothesis related to the configuration of interest in order to improve the computational process.

4.1. Configuration of interest and symmetries

The problem of interest is the case of a single three-dimensional poroelastic material bonded onto a rigid wall. The sample has a parallelepipedic shape corresponding to a large class of applications often found in the industrial and scientific literature. In those configurations it can be noticed that the original problem has internal geometrical symmetries. Consequently, during the mode computation, the internal symmetries will generate several solutions associated with the same eigenvalue. This leads to convergence problems in the numerical computation of the modes. In addition, it has been highlighted [18] that the orthogonality with respect to matrices [**A**] and [**B**] is only valid if the eigenvalues are different. The alternative is then to consider a reduced problem deduced from the initial one and taking into account the internal symmetries.

4.2. Construction of the augmented problem

4.2.1. General considerations

In order to find the modes of operator $\mathscr{D}_d$, Eq. (14) needs to be solved. As the system is large, it is essential to calculate only a selected set of eigenvalues and eigenmodes. Hence, iterative algorithms are the most appropriate for the mode computation [20]. They provide the eigenvectors corresponding to the dominant eigenvalues (i.e., eigenvalues with the largest norm). Since for the problem of interest, the eigenvalues with the lowest norm have to be computed, adapted methods (inverse power iteration method, etc.) or direct methods applied to matrix $[\mathbf{C}]^{-1}$ need to be used. They both require the inversion of matrix [**C**] whose size is nd. The following subsection presents an equivalent eigenvalue problem derived from Eq. (14) which makes the numerical computation of modes easier.

4.2.2. The modified poroelastic eigenvalue problem

The aim of this subsection is to modify the initial eigenvalue problem $[\mathbf{C}]\mathbf{U} = (\mathrm{j}\omega)\mathbf{U}$ into an equivalent one $[\mathbf{C}']\mathbf{V} = (1/\mathrm{j}\omega)\mathbf{V}$. Hence, the search for the dominant eigenvalues of the modified problem is equivalent to the search for the eigenvalues with the lowest norm of the initial problem.

The eigenvalue problem associated with Eq. (1) is equivalent to

$$\begin{bmatrix} [\mathbf{K}_{int}] + (\mathrm{j}\omega)^2\tilde{\rho}[\mathbf{M}_{int}] & -(\mathrm{j}\omega)\tilde{\gamma}[\mathbf{C}_{int}] \\ -\tilde{\gamma}[\mathbf{C}_{int}]^{\mathrm{t}} & -\dfrac{h^2}{\tilde{\rho}_{22}(\mathrm{j}\omega)}[\mathbf{H}_{int}] - \dfrac{(\mathrm{j}\omega)h^2}{\tilde{R}}[\mathbf{Q}_{int}] \end{bmatrix} \begin{Bmatrix} (\mathrm{j}\omega)\mathbf{u} \\ \mathbf{P} \end{Bmatrix} = \mathbf{0}. \tag{32}$$

Hence, if $(s, \{\mathbf{w}, \mathbf{P}\})$ is a solution of Eq. (32), $(s, \{s^{-1}\mathbf{w}, \mathbf{P}\})$ is a solution of the initial eigenvalue problem. This new formulation has the advantage of leading to an invertible $[\mathbf{M}_0]$ matrix [18]. The Taylor expansion of problem (32) reads

$$\sum_{i=0}^{d} [\mathbf{M}_i](\mathrm{j}\omega)^i\mathbf{v} + \mathscr{R}'_d(\omega)\mathbf{v} = \mathbf{0}, \tag{33}$$

with the following matrices:

$$[\mathbf{M}_0] = \begin{bmatrix} k_0[\mathbf{K}_{int}] & [\mathbf{0}] \\ -c_0[\mathbf{C}_{int}]^{\mathrm{t}} & -h_1[\mathbf{H}_{int}] \end{bmatrix}, \tag{34}$$

$$[\mathbf{M}_1] = \begin{bmatrix} [\mathbf{0}] & -c_0[\mathbf{C}_{int}] \\ -c_1[\mathbf{C}_{int}]^{\mathrm{t}} & -h_2[\mathbf{H}_{int}] - q_0[\mathbf{Q}_{int}] \end{bmatrix}, \tag{35}$$

$$[\mathbf{M}_2] = \begin{bmatrix} m_0[\mathbf{M}_{int}] & -c_1[\mathbf{C}_{int}] \\ -c_2[\mathbf{C}_{int}]^{\mathrm{t}} & -h_3[\mathbf{H}_{int}] - q_1[\mathbf{Q}_{int}] \end{bmatrix}, \tag{36}$$

$$[\mathbf{M}_i] = \begin{bmatrix} m_{i-2}[\mathbf{M}_{int}] & -c_{i-1}[\mathbf{C}_{int}] \\ -c_i[\mathbf{C}_{int}]^{\mathrm{t}} & -h_{i+1}[\mathbf{H}_{int}] - q_{i-1}[\mathbf{Q}_{int}] \end{bmatrix} \quad (i \geqslant 3), \tag{37}$$

where d corresponds to the order of Taylor expansion in terms of ω. The generalized eigenvalue problem (11) can be written as

$$(\mathrm{j}\omega)[\mathbf{A}']\mathbf{V} = [\mathbf{B}']\mathbf{V}, \quad \mathbf{V} = \begin{Bmatrix} \mathbf{v} \\ (\mathrm{j}\omega)\mathbf{v} \\ \vdots \\ (\mathrm{j}\omega)^{d-1}\mathbf{v} \end{Bmatrix}, \tag{38}$$

$$[\mathbf{A}'] = \begin{bmatrix} [\mathbf{L}'] & [\mathbf{M}_d] \\ [\boldsymbol{\Gamma}] & [\mathbf{0}] \end{bmatrix}, \quad [\mathbf{B}'] = \begin{bmatrix} -[\mathbf{M}_0] & [\mathbf{0}] \\ [\mathbf{0}] & [\boldsymbol{\Gamma}] \end{bmatrix}, \quad [\mathbf{L}'] = [\,[\mathbf{M}_1] \quad \cdots \quad [\mathbf{M}_{d-1}]\,], \tag{39}$$

which can be rewritten

$$[\mathbf{C}']\mathbf{V} = \frac{1}{(\mathrm{j}\omega)}\mathbf{V} \quad \text{with } [\mathbf{C}'] = \begin{bmatrix} -[\mathbf{M}_0]^{-1}[\mathbf{L}'] & -[\mathbf{M}_0]^{-1}[\mathbf{M}_d] \\ [\mathbf{I}_{n(d-1)}] & [\mathbf{0}] \end{bmatrix}. \tag{40}$$

The computations of the lowest modes of the initial problem (14) is then equivalent to the search for the dominant modes of Eq. (40).

4.3. Search for modes

The second step of the method is the search for the modes. Two methods of determination of the eigenvalues of similar problems were studied by Bridges and Morris [21]. In the case of interest both eigenvalues and eigenvectors are needed and as the systems are generally large, iterative algorithms are appropriate [20]. At the moment, such classical algorithms are used for this computation. Because of their generality, these procedures do not optimize the solution. Hence, there is a stake to develop an adapted algorithm for mode computation which can highly decrease the number of needed operations. The particular form of matrix $[\mathbf{C}']$ can especially be judiciously exploited.

4.4. Selection of modes

A procedure of selection was proposed in Ref. [18] which consisted of comparing the maximum value of the spectrum of excitation and the maximum frequency of the selected eigenvalues. This was based on the analytical expression of the contribution z of a given mode $\{s, \mathbf{\Phi}\}$ in the case where the modal problem is diagonal (i.e., the problem whose modes are calculated is the one on which the forcing is applied) for a poroelastic material excited by a force $\mathbf{f}$ at frequency ω. The norm of z can be expressed as the product of two terms; the space term and the frequency term. Hence,

$$|z| = \left| \frac{\boldsymbol{\psi}^{\mathrm{t}}\mathbf{f}}{\mathbf{\Phi}^{\mathrm{t}}[\mathbf{B}]\mathbf{\Phi}} \right| \times \frac{1}{|s - \mathrm{j}\omega|}. \tag{41}$$

In the former paper, only the frequency term was considered and all the space terms were considered of the same order. The ratio α_c between the maximum imaginary part of the selected eigenvalue and the frequency of excitation was defined and provides then an empirical criterion for the selection of modes. As this previous criterion of selection has no general validity, an alternative procedure can be presented in order to give an other procedure to select the modes. For the first excitation frequency, an initial α_c is taken and the modal problem is solved with the corresponding number of modes. The number can be, for example, obtained by looking to previous simulations done with similar materials. A modal solution is then obtained and converted to a temporary nodal result. The relative difference of the two members of Eq. (1) with this solution is calculated. If this residual is estimated to be sufficiently small, the temporary result is validated and the next frequency is investigated; in the other case, α_c is increased and the calculation is done until obtaining a satisfying residual.

4.5. Projection

To improve the projection process, two particular properties of the problem can be exploited. Firstly, an adapted algorithm taking into account the sparse property of the matrix of the problem issued from the finite-element discretization can decrease the time of computation of the projection. Secondly, a property of the projection family $[\boldsymbol{\psi}]_m$ can be used. Indeed, it has been observed in Ref. [18] that the numerical results are improved if the initial modes obtained by the search procedure are divided into a solid and a fluid part for the modal solution. In three-dimensional

cases, a splitting is performed by decoupling directions x, y and z. This splitting trick can be relevant only for a parallelepipedic isotropic porous material because the linearity in space of the poroelastic problem together with the particular geometry of the sample allow for it. Nevertheless, it leads to a number of projection vectors equal to four times the number of selected modes. The difference between the case where the modes are divided into two parts and the one where they are divided into four parts needs further study. The theoretical explanation of this phenomena lies in the range of computational research on numerical methods and is not the purpose of this paper. In the following, all the presented cases will correspond to a splitting into four parts. Then, for each projection vector, only the non-null coefficients corresponding to the considered direction need to be taken into account for the projection, which improves the computation.

5. Study of generalized complex modes

The purpose of this section is to use an energetic interpretation of the different calculated modes to exhibit two categories of modes. A presentation of the different expressions of the developed powers is first undertaken for an harmonic excitation at circular frequency ω. These expressions will then be adapted to a modal context and two categories of modes will finally be obtained.

5.1. General considerations

First of all, the expressions of the powers developed by the elastic and inertial forces inside the porous material at frequency ω together with the dissipated powers are recalled [22]. The time-averaged strain power and kinetic power are, respectively, given by

$$\langle \mathscr{P}_{str} \rangle = \frac{\omega}{2} \mathbf{u}^*[\mathbf{K}_{int}]\mathbf{u} + \mathscr{R}\left(\frac{h^2\omega}{2\tilde{R}}\right) \mathbf{P}^*[\mathbf{Q}_{int}]\mathbf{P}, \tag{42a}$$

$$\langle \mathscr{P}_{kin} \rangle = \frac{\omega^3}{2} \mathscr{R}(\tilde{\rho}) \mathbf{u}^*[\mathbf{M}_{int}]\mathbf{u} + \mathscr{R}\left(\frac{h^2}{2\omega\widetilde{\rho_{22}}}\right) \mathbf{P}^*[\mathbf{H}_{int}]\mathbf{P} - \mathscr{I}(\omega\tilde{\gamma})\mathscr{R}(\mathbf{u}^*[\mathbf{C}_{int}]\mathbf{P}). \tag{42b}$$

In the second expression, the first term is related to the displacement of the solid phase, the second one to the pressure of the fluid phase and the last one is a coupling term whose origin is the transformation from the $\{\mathbf{u}, \mathbf{U}\}$ formalism into $\{\mathbf{u}, P\}$ [10]. The time-averaged power dissipated can be subdivided into contributions from powers dissipated through structural damping in the skeleton, viscous and thermal effects which are, respectively, noted $\langle \mathscr{P}^s_{dis} \rangle$, $\langle \mathscr{P}^v_{dis} \rangle$, $\langle \mathscr{P}^t_{dis} \rangle$ and defined by Ref. [22].

$$\langle \mathscr{P}^s_{dis} \rangle = \frac{\omega\eta_s}{2} \mathbf{u}^*[\mathbf{K}_{int}]\mathbf{u}, \tag{43a}$$

$$\langle \mathscr{P}^v_{dis} \rangle = \underbrace{-\frac{\omega^3}{2} \mathscr{I}(\tilde{\rho}) \mathbf{u}^*[\mathbf{M}_{int}]\mathbf{u}}_{\mathscr{P}^s_{vis}} + \underbrace{\mathscr{I}\left(\frac{h^2}{2\omega\widetilde{\rho_{22}}}\right) \mathbf{P}^*[\mathbf{H}_{int}]\mathbf{P}}_{\mathscr{P}^f_{vis}} - \underbrace{\mathscr{I}(\omega\tilde{\gamma}).\mathscr{I}(\mathbf{u}^*[\mathbf{C}_{int}]\mathbf{P})}_{\mathscr{P}^{coup}_{vis}}, \tag{43b}$$

$$\langle \mathscr{P}^t_{dis} \rangle = -\mathscr{I}\left(\frac{h^2\omega}{2\tilde{R}}\right) \mathbf{P}^*[\mathbf{Q}_{int}]\mathbf{P}. \tag{43c}$$

For the time-averaged viscous dissipated powers, the same repartition is observed as for the time-averaged kinetic power.

The following subsection is devoted to the application of these expressions to the obtained modes.

5.2. Energetic interpretation of modes

5.2.1. Classification of modes

By analogy with fluid structure interaction problems, modes can be separated in two categories: 'solid controlled modes' and 'fluid controlled modes'. It can be useful to find a criterion to differentiate the two kinds of modes. It is proposed to investigate the ratio Ξ between the amplitude of the powers stored in each phase at the eigenfrequency (which corresponds to the sum of kinetic and strain powers at $\omega = \omega_i$). Fig. 1 shows the ratio of the amplitude of the power stored in the fluid phase to the one of the power stored in the solid phase for the calculated modes corresponding to a configuration which will be studied in the numerical results (material A in acoustical configuration). It can be observed that two categories of modes can be distinguished by this criterion. These sets can be separated by the empirical value $\Xi = 1$. Always by analogy with fluid structure interaction problems, modes with $\Xi > 1$ will be referred to as 'fluid controlled modes' because most of the energy is stored in the fluid phase. The second category ($\Xi < 1$) will be called 'solid controlled modes'.

5.2.2. Modal powers

The separation of modes into two categories can also be highlighted when looking at the partition of the powers dissipated by the different mechanisms when the material vibrates in a given modal shape as a function of frequency. The evolutions of these different expressions versus frequency are governed by the evolution of the tilded coefficient. Indeed, it can be observed that the modal contribution can be separated in two parts. The first one is related to the evolution versus frequency of the tilded coefficients. The second one is related to the mode shape.

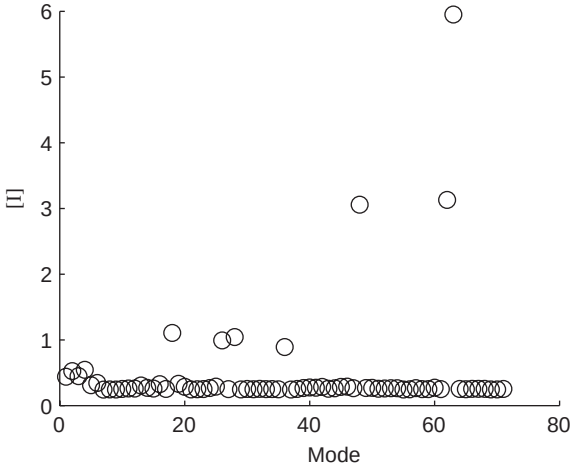

Fig. 1. Ratio of modal energies.

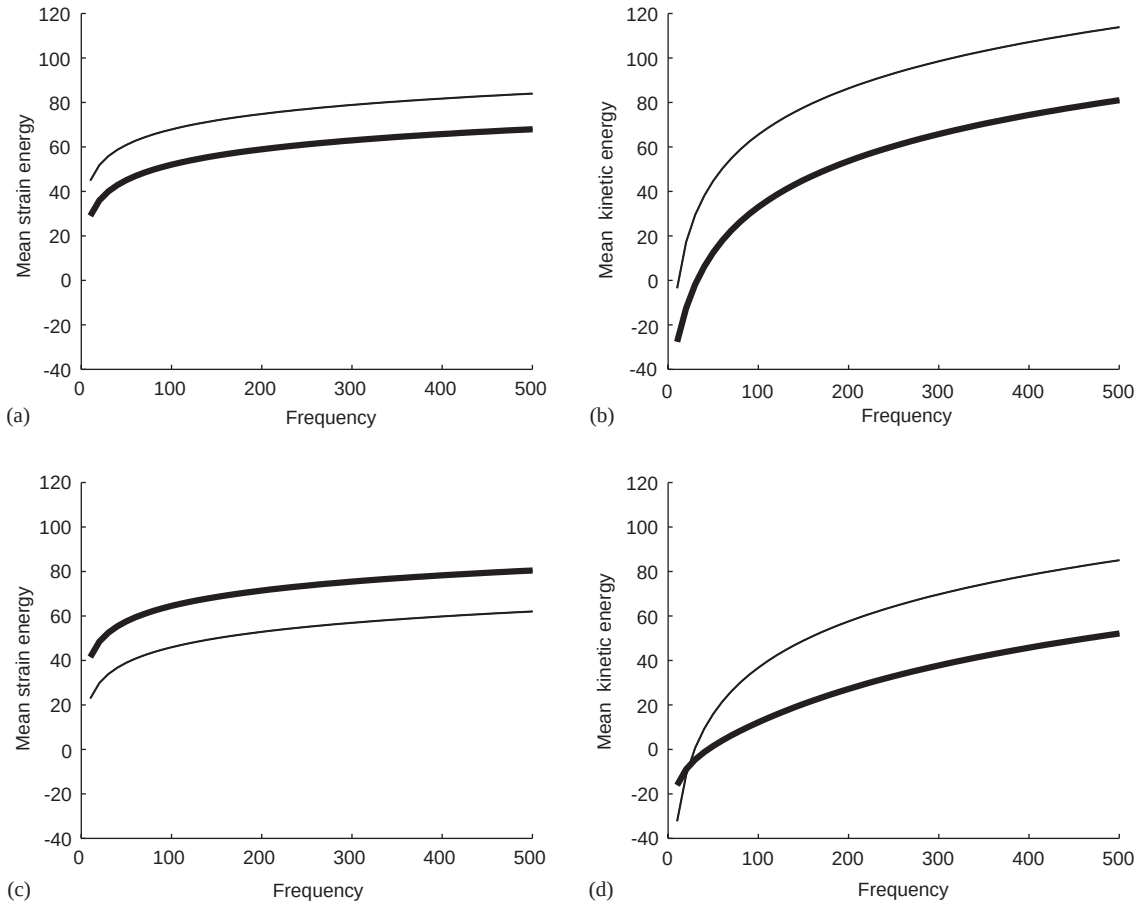

Fig. 2. (a) Solid controlled mode: mean strain energy, (b) solid controlled mode: mean kinetic energy, (c) fluid controlled mode: mean strain energy, (d) fluid controlled mode: mean kinetic energy. Thin line: solid phase; bold line: fluid phase. Unit dB ref: 10^{-12} W.

Fig. 2 shows the partition of the mean strain power and the mean kinetic power in each phase as a function of frequency for the first solid controlled mode and the first fluid controlled mode. The first observation concerns the mean strain power which is more important in the controlling phase than in the other. For the kinetic power, a difference is observed between both categories of mode but at high frequencies the modal kinetic power is more important in the solid phase in any case. On the other hand, for the fluid controlled mode, the modal kinetic power is more important in the fluid phase than in the solid phase at low frequency.

Fig. 3 presents the powers dissipated through the three phenomena given by Eq. (43) for the first solid controlled mode and the first fluid controlled mode. One can observe that the difference between the two behaviours exhibited previously is also met for the different dissipated powers. A comparison between the thermal and structural dissipations indicates that structural dissipation is most predominant for the solid controlled mode and reciprocally for the thermal dissipation in the fluid controlled mode. For the viscous dissipated power, no significant variation with the

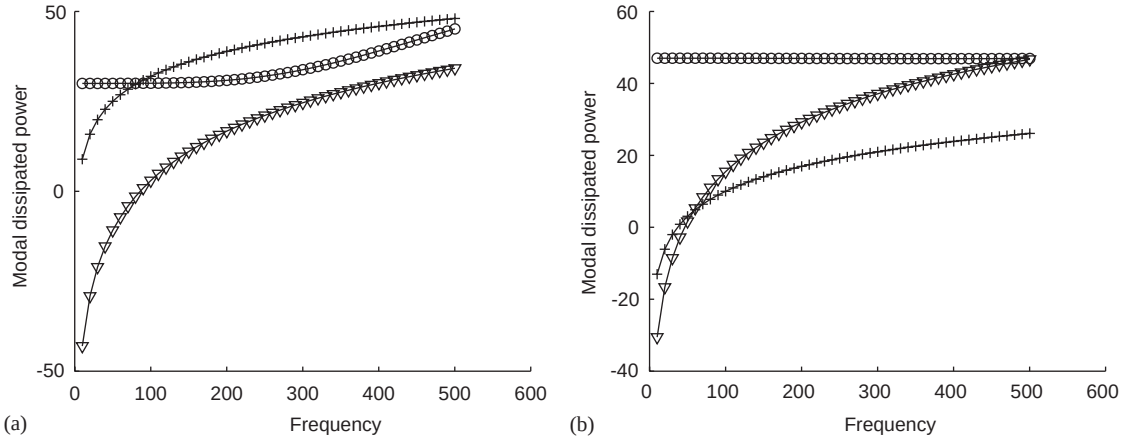

Fig. 3. Material A: (a) solid controlled mode; (b) fluid controlled mode; —+—, structural dissipated power (dB/ref: 10^{-12} W); —▽—, thermal dissipated power (dB/ref: 10^{-12} W); —○—, viscous dissipated power (dB/ref: 10^{-12} W).

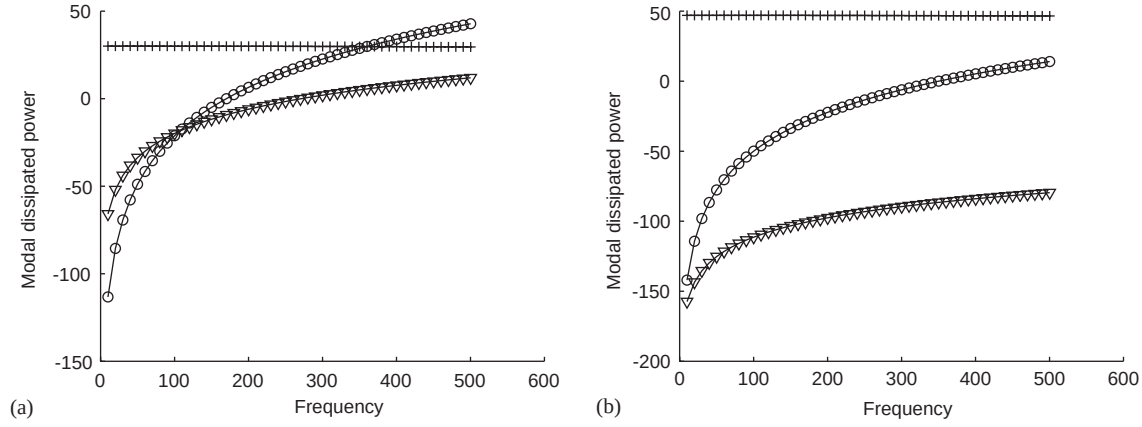

Fig. 4. Material A. Viscous dissipated power: (a) solid controlled mode; (b) fluid controlled mode; —○—, solid part (dB/ref: 10^{-12} W). —+—, fluid part (dB/ref: 10^{-12} W); —▽—, coupling term (dB/ref: 10^{-12} W).

frequency is observed for the fluid controlled mode and an increase at higher frequencies for the solid controlled mode can be observed. This can be explained by comparing the evolutions of the different terms of the viscous dissipated power. Fig. 4 presents the three parts of the viscous dissipated power as a function of frequency. The evolution of the solid part follows $(\omega^3/2)\mathcal{I}(\tilde{\rho})$ and the one of the fluid phase is governed by $\mathcal{I}(h^2/2\omega\widetilde{\rho_{22}})$. For the fluid controlled mode, $\mathscr{P}^f_{vis}$ dominates and as $\mathcal{I}(h^2/2\omega\widetilde{\rho_{22}})$ is not much frequency dependant, no significant variation is observed. For the solid controlled mode, the fluid term is dominant up to a given frequency, and then, the solid term is prevalent. The coupling term is always negligible compared to the dominant term. The evolution of the viscous dissipated power as a function of frequency can be explained: the first term ($\mathscr{P}^s_{vis}$) is prevalent but as $(\omega^3/2)\mathcal{I}(\tilde{\rho})$ tends to zero at low frequency, the modal viscous dissipated power is there governed by the fluid phase and the higher the frequency, the more preponderant the solid term becomes.

This energetic study allows for the classification of modes in two categories: the solid controlled modes and the fluid controlled modes. An analysis of the variation of the partition of the phenomena versus frequency was also initiated and confirmed the separation in two categories. The follow-up of this analysis is an extension of this paper.

6. Results

6.1. Introduction

This section is devoted to the presentation of numerical simulations. It consists of the comparison of the results obtained by a direct solution of the poroelastic problem and the ones obtained by the generalized complex modes technique for different sets of selected modes. The reference solution is first presented and the convergence of the modal approach is then investigated. The aim of this section is to show that the modal technique can decrease significantly the sizes of the systems to solve.

In Section 4.1 it was mentioned that the use of internal symmetries could be relevant. Here, all the configuration parameters and results in term of number of degrees of freedom are given without taking into account the eventual use of symmetry properties. This choice was done in order to compare the reference and the modal solution in a sound way. Nevertheless, the implementation of the modal approach was done by using as often as possible the symmetry properties described before.

Two configurations are considered. The first one, called the mechanical configuration consists of a sample of a poroelastic material bonded onto a rigid wall, with free lateral edges and excited by a rigid piston motion (a uniform normal displacement of the solid phase on the surface of excitation is imposed). The second one, called the acoustic configuration is the case of a porous medium bonded onto a rigid wall with bonded lateral edges and with an imposed uniform pressure on the surface of excitation.

Different kinds of porous materials (principally foams and wools) have been investigated. Similarities between the convergence of the method for these different materials have been

Table 1
Samples characteristics

Sample	Material A	Material B	Material C
Flow resistivity, σ (kN/m^4 s)	32	10.8	20.2
Porosity, h	0.96	0.91	0.92
Tortuosity, α_∞	1.7	1.0	1.2
Viscous characteristic length, Λ (m)	90×10^{-6}	105×10^{-6}	63.8×10^{-6}
Thermal characteristic length, Λ' (m)	165×10^{-6}	129×10^{-6}	133.8×10^{-6}
The Poisson coefficient, v	0	0.41	0
In vacuo shear's modulus, N (kPa)	84.5	76.3	185.7
Structural damping coefficient, η_s	0.1	0.1	0.1
Solid density, ρ_1 (kg/m^3)	30	8.9	92.6

observed. Their physical properties are given in Table 1 corresponding to two wools (A and C) and one foam (B).

6.2. Reference solution

The solution of the initial problem (1) is considered as the reference solution and is computed at each frequency by a direct solution of the system based on a Gauss method. In the case of interest, this solution is given by a commercial software (NOVA©Mecanum Inc. [23]). The comparison of this solution with the results obtained by the modal approach is carried out through the computation of classical vibro-acoustic indicators: the mean square velocity along the i-axis (where i correspond to x, y or z) referred to as $\langle V_i^2 \rangle$ and the mean square pressure noted $\langle P^2 \rangle$. These indicators are:

$$\langle V_i^2 \rangle = \frac{\omega^2}{2\Omega} \int_\Omega |u_i|^2 \, \mathrm{d}\Omega = \frac{\omega^2}{2\Omega} \mathbf{u}^*[\mathbf{T}_i]^{\mathrm{t}}[\mathbf{M}_{int}][\mathbf{T}_i]\mathbf{u}, \tag{44a}$$

$$\langle P^2 \rangle = \frac{1}{2\Omega} \int_\Omega |P|^2 \, \mathrm{d}\Omega = \frac{\omega^2}{2\Omega} \mathbf{P}^*[\mathbf{Q}_{int}]\mathbf{P}, \tag{44b}$$

$[\mathbf{T}_i]$ is a boolean matrix which gives the displacements along the considered direction. The dissipated powers whose expressions have been given in the previous section are also considered.

The works on the convergence of poroelastic finite elements [11,16,24] indicate that for a large range of materials an empirical criterion of convergence of the finite-element solution consists in using a size of element smaller than $\lambda/12$ (λ is the minimum value of Biot's wavelength) for a correct estimate of the amplitude of the solution in dB. In the present study, the procedure to obtain a mesh leading to a number of d.o.f.'s as small as possible is as follows. For each configuration, according to the geometrical dimensions of the problem an initial mesh is chosen corresponding to a $\lambda/6$ discretization. Then the mesh is refined until obtaining no significant variation of the vibroacoustic indicators.

6.3. Modal solutions

While investigating the method, several observations have been made. The first one is that the convergence speed depends more on the configuration (mechanic, acoustic) than on the nature of the material (wool, foam). Indeed two kinds of convergence behaviour appear, each one corresponding to a given configuration. For the mechanical configuration the convergence can be considered as classical in the sense that while increasing α_c the precision grows. For the acoustical configurations, differences occurred and problems of convergence for the indicators of the fluid phase were pointed out. Hence, it is first observed a convergence of only the indicators of the solid phase. Secondly the augmentation of α_c (i.e., the increase of the number of selected modes) did not improve significantly the results. The convergence of the fluid phase indicators together with the perfect convergence of the one of the solid phase indicators was obtained later on when increasing the number of kept modes.

To illustrate this, four different simulations are presented here, each one is a sample of the observed results in the numerical simulations. The dimensions of the samples and the mesh

Table 2
Geometry and meshes

Sample	Material A	Material B	Material C
Biot wavelength $P1$(500 Hz) (cm)	40.2	34.0	20.1
Biot wavelength $P2$(500 Hz) (cm)	25.9	30.9	4.5
Biot wavelength S(500 Hz) (cm)	20.5	10.6	3.2
L_x (cm)	15	15	10
L_y (cm)	10	10	10
L_z (cm)	5	5	5
Theoretical number of nodes (x)	9	17	19
Theoretical number of nodes (y)	6	12	19
Theoretical number of nodes (z)	3	6	7
Chosen number of nodes (x)	10	15	15
Chosen number of nodes (y)	8	10	12
Chosen number of nodes (z)	6	7	6

obtained with the discretization process described in Section 6.2 are given in Table 2. The convergence of the generalized complex mode technique in each of these cases is investigated in the following section.

6.3.1. *Material B in mechanical configuration*

Fig. 5 shows the values of the vibro-acoustic indicators in dB versus frequency and depicts the response of a sample of material B in a mechanical configuration in the frequency range [0; 500 Hz]. This material corresponds to an elastic foam. It can be observed in Table 2 that this number of nodes is of the same order as the one given by the criterion given by the literature [11,24]. This leads to a 1572 d.o.f. problem. In this case, the number of d.o.f. allowing one to achieve the convergence of the solution significantly decrease when the modal technique is used. Sixty-four d.o.f. corresponding to a selection of 15 modal shapes ($\alpha_c = 2.5$) are sufficient. Note that even a 24 d.o.f. problem corresponding to a selection of 5 modal shapes ($\alpha_c = 1.5$) can be considered as acceptable. There is quite a good estimation of the total dissipated power and pressure and velocity along the z-axis. For the dissipation properties, only 24 d.o.f.'s are sufficient.

6.3.2. *Material C in mechanical configuration*

Fig. 6 shows the values of the vibro-acoustic indicators in dB versus frequency and displays the response of a sample of material C in a mechanical configuration in the frequency band [10–500 Hz]. This material corresponds to a wool. Its Poisson's ratio is zero and its Young's modulus is higher than the one of material B. The mesh needed to achieve the convergence of the solution leads to a 3582 d.o.f. problem. The process of convergence of the generalized complex modes is comparable to the former case. One can see that the number of degrees of freedom needed to obtain an accurate result with the modal approach is 124 which corresponds to keeping 30 modal shapes ($\alpha_c = 3.2$) in the modal expansion. The decrease is here also quite important. In this case, even a 84 d.o.f. problem corresponding to a 20 modes selection ($\alpha_c = 2.1$) can be considered as

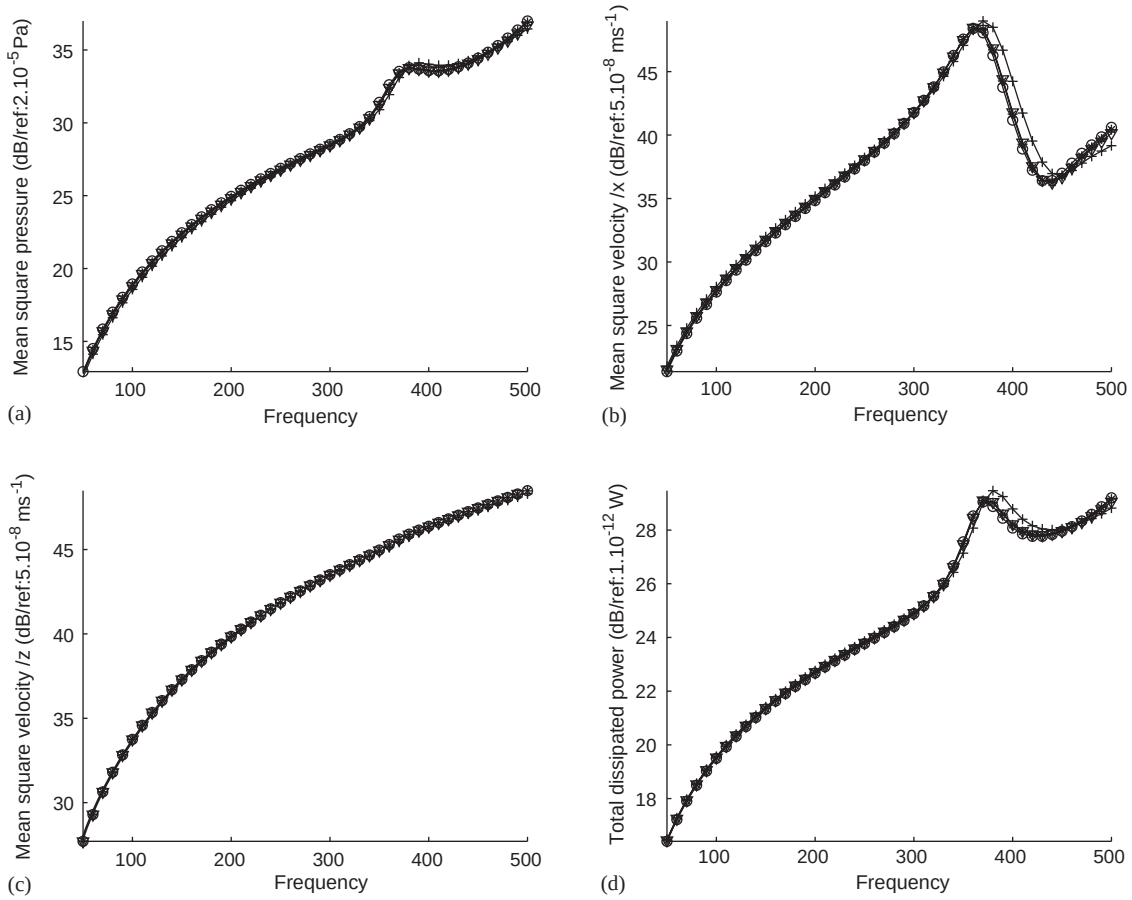

Fig. 5. Material B. Mechanical excitation: (a) mean square pressure, (b) mean square velocity along x-axis, (c) mean square velocity along z-axis, (d) total dissipated power. —○—, exact (1572 d.o.f.'s); —+—, 24 d.o.f.'s; —▽—, 44 d.o.f.'s; —∗—, 64 d.o.f.'s.

acceptable. This is another case where a modal treatment of the problem is well appropriated. For mechanical configurations, it is proposed empirically and as an estimate to consider α_c around 3.

6.3.3. *Materials A and B in acoustical configuration*

Consider now the acoustical configuration. Fig. 7 shows the values of the vibro-acoustic indicators in dB versus frequency and depicts the response of a sample of material A in the frequency range [10; 500 Hz]. 3030 d.o.f.'s are needed to obtain the convergence of the finite element model. As discussed in the general considerations section, the convergence of the method can be divided in three parts. The first one is the convergence of the indicators of the solid phase but without interesting results regarding to the fluid phase. The second part is the addition of modes without any noticeable improvements neither in the solid phase nor in the fluid phase and finally, the addition of further modes leads to the acquisition of accurate results. Consequently, there were two distinct phases of convergence and by looking at the classification of modes done in the previous section, it appears that they, respectively, correspond to the addition of solid

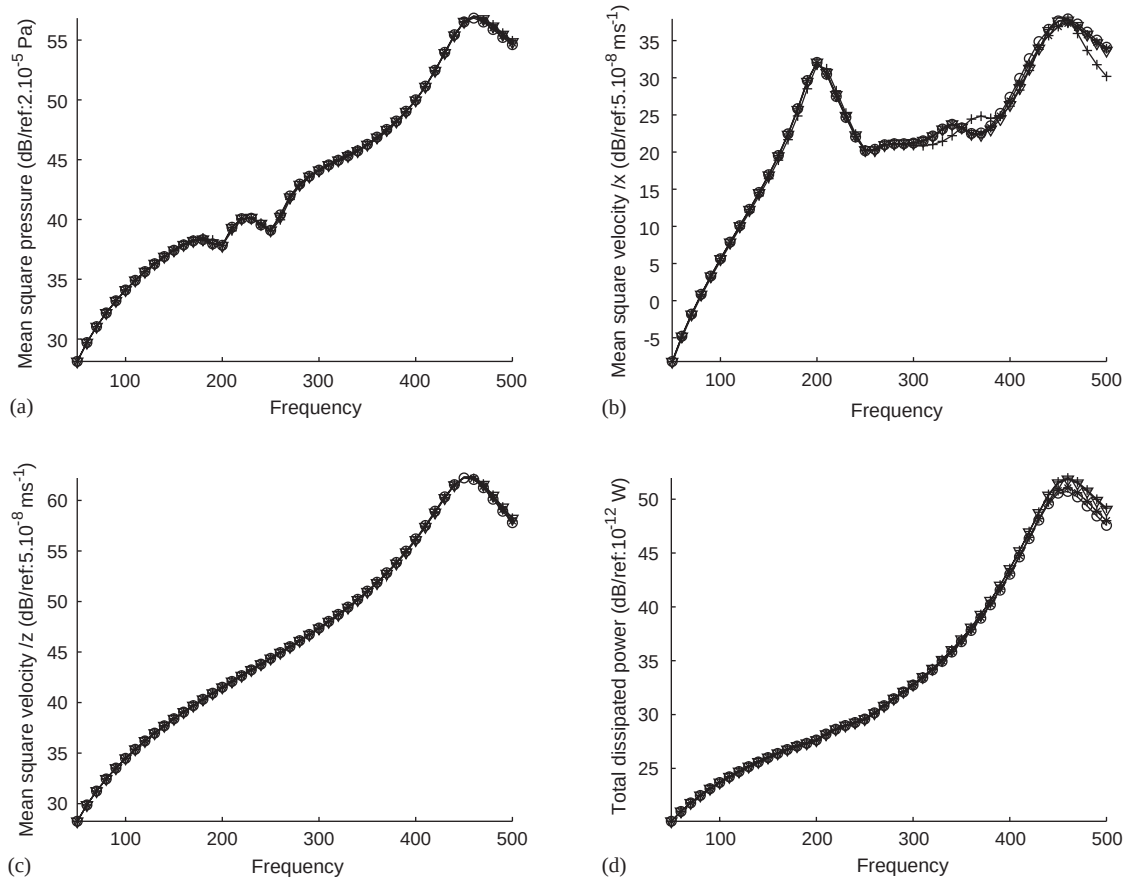

Fig. 6. Material C. Mechanical excitation: (a) mean square pressure, (b) mean square velocity along x-axis, (c) mean square velocity along z-axis, (d) total dissipated power. —○—, exact (5582 d.o.f.'s); —+—, 44 d.o.f.'s; —▽—, 84 d.o.f.'s; —∗—, 124 d.o.f.'s.

controlled modes (the first ones) and of fluid controlled modes (second ones). Hence it seems that the energetic interpretation can be used judiciously to improve the process of selection. The idea is then to consider differently the solid controlled and fluid controlled modes and for each category to give a corresponding critical parameter α_c^s and α_c^f for, respectively, the solid and fluid modes. A user will then select the solid controlled modes whose imaginary part of the eigenvalue is lower than $\alpha_c^s \omega_{max}$ and the fluid controlled modes with $\omega_i < \alpha_c^f \omega_{max}$ where ω_{max} is the maximum frequency of the spectrum of excitation.

By recalling the numerical results on material A; the convergence of the solid modes improves up to a limit value corresponding to $\alpha_c^s = 1.3$ (i.e., 84 d.o.f. or 20 modal shapes). While increasing α_c^s, additional solid modes are selected but no significant improvement in the convergence process occurs. It can be seen that the convergence is good for the velocity indicators but limited for the mean square pressure and the absorption coefficient. The idea is now to use the new process of selection which separates solid controlled and fluid controlled modes. The addition of the fluid

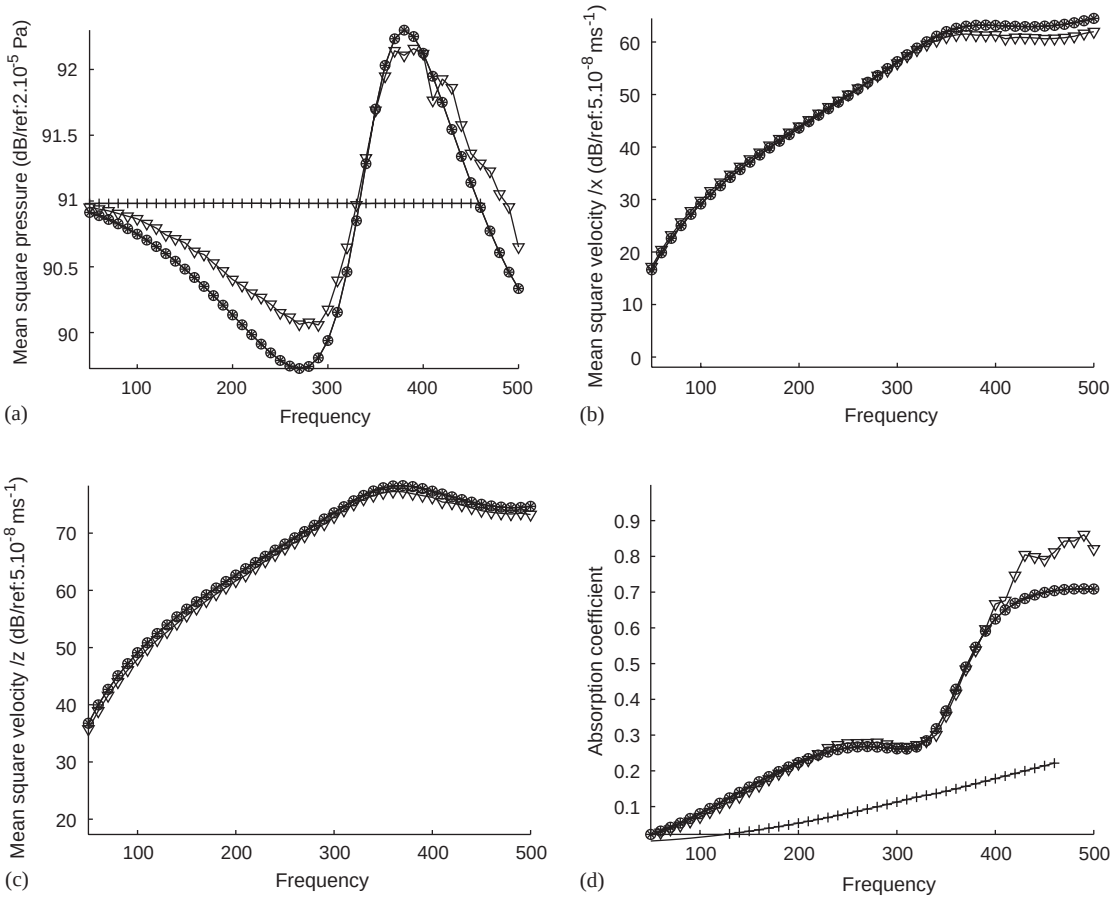

Fig. 7. Material A. Acoustical excitation: (a) mean square pressure, (b) mean square velocity along x-axis, (c) mean square velocity along z-axis, (d) absorption coefficient. —○—, exact (3030 d.o.f.'s); —▽—, solid modes (84 d.o.f.'s); —∗—, solid modes and fluid modes (124 d.o.f.'s).

modes controlled improves the convergence up to $\alpha_c^f = 4.2$ corresponding to a total of 124 d.o.f. It is interesting to note that not all the solid controlled modes with $\omega_r < \alpha_c^f \omega_{max}$ were selected. Some of them were discarded without penalizing the convergence of the solution.

Fig. 8 displays similar results for the application of the technique to the calculation of the response of a sample of material B in an acoustical configuration. 7944 d.o.f. are here needed to obtain the convergence of the finite-element model. The same observations as before can be done. Only the selected solid modes corresponding to a $\alpha_c^s = 1.9$ give an accurate results for the solid indicators but to obtain a good accuracy on the fluid indicators, one has to select additional fluid modes. A selection corresponding to $\alpha_c^f = 5.6$ (208 modes) gives accurate results.

These two examples show the validity of the application of the generalized complex mode technique to acoustical cases. Nevertheless, the procedure of selection was modified by distinguishing the solid controlled and fluid controlled modes. This does not seem to be necessary in the case of mechanical configurations. For these configurations, it is proposed empirically and as an estimate to consider α_c^s around 2 and α_c^f around 5.

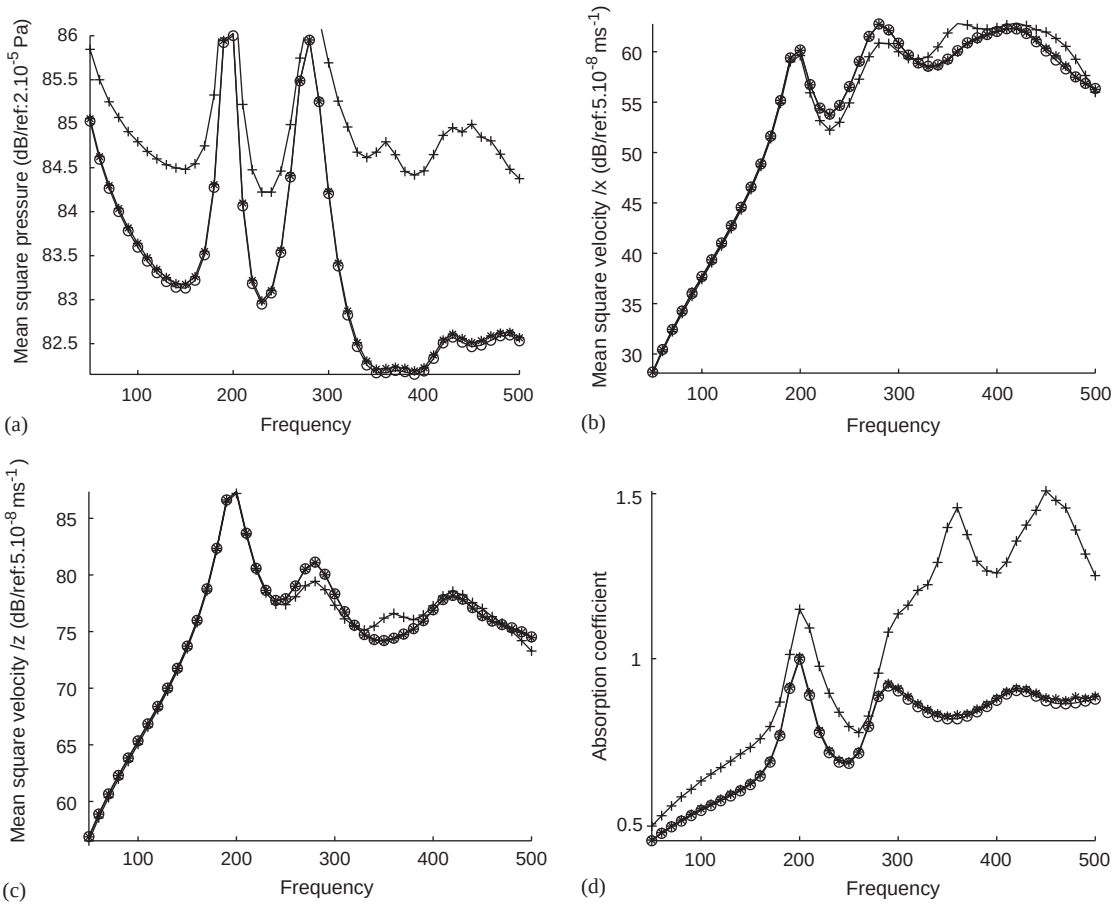

Fig. 8. Material B. Acoustical excitation: (a) mean square pressure, (b) mean square velocity along x-axis, (c) mean square velocity along z-axis, (d) absorption coefficient. —○—, exact (7944 d.o.f.'s); —+—, solid modes (64 d.o.f.'s); —∗—, solid modes and fluid modes (208 d.o.f.'s).

7. Conclusion

This paper presented the application of the generalized complex mode theory to the calculation of the forced response of a three-dimensional poroelastic material subjected to acoustical and mechanical excitations.

The first part described analytical and numerical contributions. In particular, the theoretical stability of the solution has been proved. Numerical improvements as the construction of the augmented problem and projection of the initial system on the modal family were then described.

The second part was dedicated to the numerical aspects and to the obtained results. An investigation of the different modal powers has first been performed. This enabled one to obtain informations on the different modes and to classify them in two categories: the one controlled by the solid phase and the other ones controlled by the fluid phase. A new selection procedure was

then deduced from this distinction. Numerical results obtained by the modal technique have been successfully compared to those computed by a direct solution of the finite element system. In particular, two configurations, called mechanical and acoustical, have been considered. The mechanical one leads to accurate results with the original procedure of selection. The acoustic configuration does not converge in the same way and leads to accurate results with the new selection procedure. With such a procedure of selection it was observed that the method leads to a significant reduction of the number of d.o.f. of the systems.

As the reduction is significant, the procedure for the calculation of modes now needs to be improved by taking advantage of all the analytical properties of the general eigenvalue problem. Further work involves applying this technique to multi-layered structures involving poroelastic materials.

Appendix A. Supplementary calculations

First rewrite the different terms of Eq. (24). By using the expression of matrix $[\mathbf{C}_{int}]$, one has

$$-\hat{\gamma}\frac{\hat{1}}{\rho_{22}}\mathbf{u}^*[\mathbf{C}_{int}]\mathbf{P} = \mathscr{C}^s_{dyn} - \mathscr{C}_{coup}, \tag{A.1a}$$

where

$$\mathscr{C}^s_{dyn} = s^2\int_\Omega\left(\frac{\widehat{\rho_{12}}}{\rho_{22}}u^*U + \frac{\widehat{\rho_{12}}}{\rho_{22}}\frac{\widehat{\rho_{12}}}{\rho_{22}}u^*u\right)\mathrm{d}\Omega, \tag{A.1b}$$

and

$$\mathscr{C}_{coup} = s^2\int_\Omega\left(\frac{\hat{Q}}{R}\left(u^*U + \frac{\widehat{\rho_{12}}}{\rho_{22}}u^*u\right)\right)\mathrm{d}\Omega. \tag{A.1c}$$

Eq. (24) is now multiplied by $\widehat{\rho_{22}}$ defined by Eq. (27) to give

$$\underbrace{\mathbf{u}^*[\mathbf{K}_{int}]\mathbf{u}}_{\mathscr{K}} + \underbrace{s^2\hat{\rho}\mathbf{u}^*[\mathbf{M}_{int}]\mathbf{u} + \widehat{\rho_{22}}\mathscr{C}^s_{dyn}}_{\mathscr{M}} - \widehat{\rho_{22}}\mathscr{C}_{coup} = 0, \tag{A.2}$$

with

$$\mathscr{K} = \int_\Omega\left(\boldsymbol{\sigma}^s(\widehat{u,U}) - \frac{\hat{Q}}{R}\boldsymbol{\sigma}^f(\widehat{u,U})\right) : \boldsymbol{\epsilon}^s(u)\,\mathrm{d}\Omega, \tag{A.3a}$$

and

$$\mathscr{M} = \int_\Omega\left(\widehat{\rho'_{11}}u^*u + \widehat{\rho_{22}}\frac{\widehat{\rho_{12}}}{\rho_{22}}u^*U\right)\mathrm{d}\Omega, \tag{A.3b}$$

with the definition of $\widehat{\rho'_{11}}$ recalled in Eq. (27).

The first term of Eq. (25) is equal to

$$\frac{\bar{\hat{1}}}{\rho_{22}}\hat{\gamma}\mathbf{P}^*[\mathbf{C}_{int}]^{\mathrm{t}}\mathbf{u} = \overline{\mathscr{C}_{coup}} - \mathscr{C}^f_{dyn}, \tag{A.4}$$

$$\mathscr{C}^{f}_{dyn} = \frac{\widehat{\rho_{12}}}{\rho_{22}}\overline{s^2}\int_{\Omega}\left(U^*u + \overline{\frac{\widehat{\rho_{12}}}{\rho_{22}}}u^*u\right)\mathrm{d}\Omega. \tag{A.5}$$

Then, definition (19) gives

$$\frac{h^2}{s^2}\frac{\hat{1}}{\rho_{22}}\frac{\bar{\hat{1}}}{\rho_{22}}\nabla P^*\nabla P = \overline{s^2}\left(U^*U + \overline{\frac{\widehat{\rho_{12}}}{\rho_{22}}}u^*U\right) + \mathscr{C}^{f}_{dyn}. \tag{A.6}$$

On the other hand, the constitutive law of the fluid phase (20b) yields to

$$h^2\frac{\bar{\hat{1}}}{\rho_{22}}\frac{\hat{1}}{R}P^*.P = \frac{\bar{\hat{1}}}{\rho_{22}}\underbrace{\overline{\boldsymbol{\sigma}^{f}(\widehat{u,U}):\left(\boldsymbol{\epsilon}^{f}(U) + \frac{\hat{Q}}{R}\boldsymbol{\epsilon}^{s}(u)\right)}}_{\mathscr{K}^{f}}. \tag{A.7}$$

The conjugate of Eq. (25) multiplied by $\widehat{\rho_{22}}$ defined by Eq. (27) leads to

$$\widehat{\rho_{22}}\mathscr{C}_{coup} + \int_{\Omega}\widehat{\rho_{22}}\left(U^*U + \frac{\widehat{\rho_{12}}}{\rho_{22}}U^*u\right)\mathrm{d}\Omega + \int_{\Omega}\mathscr{K}_f\,\mathrm{d}\Omega = 0. \tag{A.8}$$

The sum of equation and Eqs. (A.2) and (A.8) yields

$$-\Gamma_{kin} + \Gamma_{def} = 0, \tag{A.9a}$$

$$\Gamma_{kin} = -s^2\int_{\Omega}\left(\widehat{\rho'_{11}}u^*u + \widehat{\rho_{22}}\frac{\widehat{\rho_{12}}}{\rho_{22}}(u^*U + U^*u) + \widehat{\rho_{22}}U^*U\right)\mathrm{d}\Omega, \tag{A.9b}$$

$$\Gamma_{def} = \int_{\Omega}(\boldsymbol{\sigma}^{s}(\widehat{u,U}):\boldsymbol{\epsilon}^{s}(u^*) + \boldsymbol{\sigma}^{f}(\widehat{u,U}):\boldsymbol{\epsilon}^{f}(U^*))\,\mathrm{d}\Omega. \tag{A.9c}$$

Appendix B. Rewriting $s^2\Gamma_{kin}$

One has

$$-s^2\mathscr{I}_k = s^2\left(\widehat{\rho'_{11}} + \widehat{\rho_{22}}\frac{\widehat{\rho_{12}}}{\rho_{22}}\right)|u|^2 + \left(\widehat{\rho_{22}} + s^2\widehat{\rho_{22}}\frac{\widehat{\rho_{12}}}{\rho_{22}}\right)|U|^2 - s^2\widehat{\rho_{22}}\frac{\widehat{\rho_{12}}}{\rho_{22}}|u-U|^2. \tag{B.1}$$

The sign of the real and imaginary parts of each one of these terms is now investigated. This sign can be obtained by looking at the one of the first order terms. One has

$$\left(\widehat{\rho'_{11}} + \widehat{\rho_{22}}\frac{\widehat{\rho_{12}}}{\rho_{22}}\right) = \rho_{11} + O\left(\left|\frac{s}{H}\right|^2\right), \tag{B.2a}$$

$$\left(\widehat{\rho_{22}} + \widehat{\rho_{22}}\frac{\widehat{\rho_{12}}}{\rho_{22}}\right) = \rho_{22} + O\left(\left|\frac{s}{H}\right|^2\right), \tag{B.2b}$$

$$s\widehat{\rho_{22}}\frac{\widehat{\rho_{12}}}{\rho_{22}} = -\sigma h^2 - \frac{\sigma h^2}{2}\frac{s}{H} + \rho_{12}s + O\left(\left|\frac{s}{H}\right|^2\right). \tag{B.2c}$$

σ is the flow resistivity and is positive. One can rewrite

$$s^2\left(\widehat{\rho'_{11}}+\widehat{\rho_{22}}\frac{\widehat{\rho_{12}}}{\rho_{22}}\right)=\rho_{11}s^2+s^2\left|\frac{s}{H}\right|^2(r_{11}(s)+\mathrm{j}i_{11}(s)), \tag{B.3}$$

$$s^2\left(\widehat{\rho_{22}}+\widehat{\rho_{22}}\frac{\widehat{\rho_{12}}}{\rho_{22}}\right)=\rho_{22}s^2+s^2\left|\frac{s}{H}\right|^2(r_{22}(s)+\mathrm{j}i_{22}(s)), \tag{B.4}$$

$$-s^2\widehat{\rho_{22}}\frac{\widehat{\rho_{12}}}{\rho_{22}}=\sigma h^2 s+\frac{\sigma h^2}{2H}s^2-\rho_{12}s^2+s\left|\frac{s}{H}\right|^2(r_{12}(s)+\mathrm{j}i_{12}(s)), \tag{B.5}$$

with r_{11}, i_{11}, r_{22}, i_{22}, r_{12}, i_{12} real functions of s which are all $O(1)$. Hence, the first term of $s^2\mathscr{I}_k$ is

$$s^2\underbrace{\left(\rho_{11}+\left|\frac{s}{H}\right|^2 r_{11}(s)\right)}_{\in\,\mathbb{R}^+}|u|^2+s^2\left(\underbrace{\mathrm{j}\left|\frac{s}{H}\right|^2 i_{11}(s)}_{\in O(|\frac{s}{H}|)}\right)|u|^2. \tag{B.6}$$

A similar expression is obtained for the second term. For the last one, it is recalled that $\rho_{12}<0$ and

$$\underbrace{\left(\frac{\sigma h^2}{2H}-\rho_{12}\right)|u-U|^2}_{\in\mathbb{R}^+}s^2+\left(\underbrace{\sigma h^2+\left|\frac{s}{H}\right|^2 r_{12}(s)}_{\in\mathbb{R}^+}+\mathrm{j}\underbrace{\left|\frac{s}{H}\right|^2 i_{12}(s)}_{\in\,O\left(\frac{s}{H}\right)^2}\right)\underbrace{|u-U|^2}_{\in\,\mathbb{R}^+}s. \tag{B.7}$$

Hence,

$$-s^2\mathscr{I}_k=s^2m_{11}(s)|u|^2+s^2m_{22}(s)|U|^2+s^2m_{12}(s)|U-u|^2+sc_{12}(s)|U-u|^2, \tag{B.8}$$

with the four functions $m_{11}(s)$, $m_{12}(s)$, $m_{22}(s)$, $c_{12}(s)$ so that the real is positive and the imaginary part is $O(|s/H|)^2$.

Γ_{kin} is then so that

$$-\Gamma_{kin}=s^2m(s)+sc_{kin}(s), \tag{B.9}$$

with m and c_{kin} functions of s with a positive real part and an imaginary part in $O(|s/H|)^2$.

Appendix C. Rewriting Γ_{def}

For $\mathscr{I}_d$, a similar result is obtained by using the constitutive laws (20a) and (20b). $\widehat{K_f}$ is introduced by

$$\widehat{K_f}=\frac{1}{\widehat{h1/R}}, \tag{C.1}$$

and the constitutive laws are multiplied by $h\widehat{K_f}$. Hence,

$$\boldsymbol{\sigma}^s\widehat{(u,U)}=h\widehat{K_f}\frac{\hat{A}}{R}\nabla\cdot u\mathbb{I}+2N\boldsymbol{\epsilon}^s(u)+h\widehat{K_f}\frac{\hat{Q}}{R}\nabla\cdot U\mathbb{I}, \tag{C.2a}$$

$$\boldsymbol{\sigma}^{f}\widehat{(\boldsymbol{u},\boldsymbol{U})} = h\widehat{K_f}\nabla\cdot U\mathbb{I} + h\widehat{K_f}\frac{\hat{Q}}{R}\nabla\cdot u\mathbb{I}. \tag{C.2b}$$

The contracted product by, respectively, $\boldsymbol{\epsilon}^{s}(u^{*})$ and $\boldsymbol{\epsilon}^{f}(U^{*})$ yields

$$\boldsymbol{\sigma}^{s}\widehat{(\boldsymbol{u},\boldsymbol{U})}:\boldsymbol{\epsilon}^{s}(u^{*}) = h\widehat{K_f}\frac{\hat{A}}{R}\nabla\cdot u\nabla\cdot u^{*} + 2N\boldsymbol{\epsilon}^{s}(u):\boldsymbol{\epsilon}^{s}(u^{*}) + h\widehat{K_f}\frac{\hat{Q}}{R}\nabla\cdot U\nabla\cdot u^{*}, \tag{C.3a}$$

$$\boldsymbol{\sigma}^{f}\widehat{(\boldsymbol{u},\boldsymbol{U})}:\boldsymbol{\epsilon}^{f}(u^{*}) = h\widehat{K_f}\nabla\cdot U\nabla\cdot U^{*} + h\widehat{K_f}\frac{\hat{Q}}{R}\nabla\cdot u\nabla\cdot U^{*}. \tag{C.3b}$$

By recalling Eq. (22), one obtains

$$\mathscr{I}_{def} = \underbrace{2N\boldsymbol{\epsilon}^{s}(u):\boldsymbol{\epsilon}^{s}(u^{*})}_{\in\,\mathbb{R}^{+}} + \underbrace{2N\frac{v}{(1-2v)}|\nabla\cdot u|^{2}}_{\in\,\mathbb{R}^{+}} + h\widehat{K_f}\underbrace{\left|\frac{1-h}{h}\nabla\cdot u + \nabla\cdot U\right|^{2}}_{\in\,\mathbb{R}^{+}}. \tag{C.4}$$

The first terms of $\widehat{K_f}$ are

$$\widehat{K_f} = \underbrace{P_0}_{\in\,\mathbb{R}^{+}} + \underbrace{\frac{2(\gamma-1)}{\gamma}}_{\in\,\mathbb{R}^{+}}\frac{s}{H'} + O\left(\frac{s}{H'}\right)^{2}. \tag{C.5}$$

Finally, Γ_{def} can be written as

$$\Gamma_{def} = k_0 + sc_d + r_k(s) + \mathrm{j}i_k(s). \tag{C.6}$$

k and c_d in $\mathbb{R}^{+}$ and both real functions of r_k and i_k in $O(|s/H'|)^{2}$.

References

[1] M.A. Biot, Theory of propagation of elastic waves in a fluid-saturated porous solid. I. Low frequency range, Journal of the Acoustical Society of America 28 (1956) 168–178.

[2] D.L. Johnson, J. Koplik, R. Dashen, Theory of dynamic permeability and tortuosity in fluid-saturated porous media, Journal of Fluid Mechanics 176 (1987) 379–402.

[3] Y. Champoux, Etude Expérimentale du Comportement Acoustique des Matériaux Poreux à Structure Rigide, Ph.D. Thesis, Carleton University, Ottawa, 1991.

[4] J.F. Allard, Propagation of Sound in Porous Media, Modelling Sound Absorbing Materials, Elsevier Application Science, New York, 1993.

[5] Y.J. Kang, J.S. Bolton, Finite element modeling of isotropic elastic porous materials coupled with acoustical finite elements, Journal of the Acoustical Society of America 98 (1995) 635–643.

[6] J.P. Coyette, H. Wynendaele, A finite element model for predicting the acoustic transmission characteristics of layered structures, in: S. Bolton, R.J. Bernhard (Eds.), Proceedings of Inter-Noise 95, Noise Control Foundation, Poughkeepsie, NY, 1995, pp. 1279–1282.

[7] R. Panneton, N. Atalla, An efficient finite element scheme for solving the three-dimensional poroelasticity problem in acoustics, Journal of the Acoustical Society of America 101 (1997) 3287–3298.

[8] P. Göransson, A 3d, symmetric finite element formulation of the Biot equations with application to acoustic wave propagation through an elastic porous medium, International Journal for Numerical Methods in Engineering 41 (1998) 167–192.

[9] S. Gorog, R. Panneton, N. Atalla, Mixed displacement pressure formulation for acoustic anisotropic open porous media, Journal of Applied Physics 82 (1997) 4192–4197.

[10] N. Atalla, R. Panneton, P. Debergue, A mixed displacement–pressure formulation for poroelastic materials, Journal of the Acoustical Society of America 104 (1998) 1444–1452.
[11] P. Debergue, R. Panneton, N. Atalla, Boundary conditions for the weak formulation of the mixed (u,P) poroelasiticity problem, Journal of the Acoustical Society of America 104 (1999) 2383–2390.
[12] N.-E. Horlin, M.Nordstrogm, P. Goransson, A 3-D hierarchical FE formulation of Biot's equations for elasto-acoustic modelling of porous media, Journal of Sound and Vibration 182 (2000) 479–494 doi:10.1006/jsvi.2000.3556.
[13] S. Rigobert, Modélisation par Éléments Finis des Systèmes Élasto-poro-acoustiques Couplés, Eléments Hierarchiques, Maillages Incompatibles, Modèles Simplifiés, Ph.D. Thesis, Institut National des Sciences Appliquées de Lyon, Université de Sherbrooke, 2001.
[14] D. Pilon, Influence des Conditions aux Limites sur les Mesures Acoustiques au Tube à ondes stationnaires, Master Thesis, Université de Sherbrooke, Québec, 2001.
[15] F. Sgard, N. Atalla, R. Panneton, A mixed wave-finite element approach for solving Biot's poroelasticity equations in acoustics, 16th International Congress on Acoustics/135th Meeting of the Acoustical Society of America, Seattle, WA, 1998.
[16] R. Panneton, Modélisation Numérique Tridimensionelle par Éléments Finis des Milieux Poroélastiques, Ph.D. Thesis, Université de Sherbrooke, Québec, 1996.
[17] F. Sgard, N. Atalla, R. Panneton, A modal reduction technique for the finite element formulation of Biot's poroelasticity equations in acoustics applied to multilayered structures, 16th International Congress on Acoustics/135th Meeting of the Acoustical Society of America, Seattle, USA, 1998.
[18] O. Dazel, F. Sgard, C.-H. Lamarque, N. Atalla, An extension of complex modes for the resolution of finite-element poroelastic problems, Journal of Sound and Vibration 253 (2002) 421–445.
[19] W.J. Duncan, R.A. Fraser, A.R. Collar, Elementary Matrices and Some Applications to Dynamics and Differential Equations, Cambridge University Press, Cambridge, 1938, p. 289.
[20] F. Chatelin, Valeurs Propres de Matrices, Masson, Paris, 1988.
[21] T.J. Bridges, P.J. Morris, Differential eigenvalue problems in which the parameter appears nonlinearly, Journal of Computational Physics 55 (1984) 437–460.
[22] F. Sgard, N. Atalla, J. Nicolas, A numerical model for the low-frequency diffuse field sound transmission loss of double-wall sound barriers with elastic porous lining, Journal of the Acoustical Society of America 108 (2000) 2865–2872.
[23] Nova, Mecanum Numerical Software Inc, Québec.
[24] N. Dauchez, S. Sahraoui, N. Atalla, Convergence of poroelastic finite elements based on Biot displacement formulation, Journal of the Acoustical Society of America 109 (2001) 33–40.